Estimation of line tension and contact angle from heterogeneous nucleation experimental data

A. I. Hienola[a)]
Department of Physical Sciences, University of Helsinki, Gustaf Hällströmin katu 2, FIN-00014, Helsinki, Finland

P. M. Winkler and P. E. Wagner
Institut für Experimentalphysik, Universität Wien, Boltzmanngasse 5, A-1090 Wien, Austria

H. Vehkamäki, A. Lauri, I. Napari, and M. Kulmala
Department of Physical Sciences, University of Helsinki, Gustaf Hällströmin katu 2, FIN-00014, Helsinki, Finland

(Received 8 December 2006; accepted 16 January 2007; published online 6 March 2007)

Using the classical nucleation theory corrected with line tension and experimental data of heterogeneous nucleation of *n*-nonane, *n*-propanol, and their mixture on silver particles of three different sizes, the authors were able to estimate the line tensions and the microscopic contact angles for the above mentioned systems. To do this they applied generalized Young's equation for the line tension and calculated the interfacial tensions using Li and Neumann's equation [Adv. Colloid Interface Sci. **39**, 299 (1992)]. It has been found that, for both unary and binary systems, the line tension is negative and the resulting microscopic contact angle derived from experimental nucleation data is most of the time larger than the macroscopic one. This is in contrast to earlier studies where the influence of line tension has not been accounted for. The values of the three phase contact line tension obtained in this way are of the same order of magnitude as the estimations for other systems reported in literature. The line tension effect also decreases considerably the nucleation barrier. © *2007 American Institute of Physics*. [DOI: 10.1063/1.2565769]

I. INTRODUCTION

Aerosol and cloud drop formation in the atmosphere can be initiated by heterogeneous nucleation on soluble or insoluble particles.[1] Heterogeneous nucleation has been extensively investigated in literature[2–7] and new theories have been developed.[8,9] Nevertheless, the classical heterogeneous nucleation theory (CNT) by Fletcher[10] remains the only practical approach for atmospheric models. Heterogeneous nucleation is a complex process and the relatively simplistic original classical theory often fails to explain the experimental results.[11] For instance, the characteristics of the substrate and the particular interaction between the substrate and the condensed phase have to be taken into account for a complete characterization of the critical nucleus. This can be done by introducing in the calculations the microscopic contact angle which characterizes the balance between interfacial free energies. The coexistence locus of the three phases is a line which has an excess free energy per unit length, or line tension τ, associated with it. The line tension is usually a small quantity with typical values between 10^{-13} and 10^{-5} N deduced from contact angle measurements, and it can be either negative or positive. The line tension has considerable relevance in, for example, the stability of spherical particles at liquid/fluid interfaces and wetting phenomena,[12] soap films,[13,14] and membrane stability.[15]

Gretz[16] was the first to realize the importance of line tension in heterogeneous nucleation. He included the line tension effect in the classical nucleation scheme, but his analysis was not complete. Navascues and Mederos[17] used the classical nucleation theory including line tension to analyze unary heterogeneous nucleation experimental data for water on mercury and chromous iodide on quartz. They found an almost constant microscopic contact angle for both systems, but the line tension varied with temperature. Lazaridis[18] found that the inclusion of the concepts of negative line tension and surface diffusion in the original classical theory gives a more realistic model for the heterogeneous nucleation and improves the quantitative agreement with the experimental results of the nucleation of water and water-sulfuric acid than the classical theory. Lazaridis also found that the use of line tension leads to a smaller contact angle than the macroscopic one. Padilla and Talanquer[19] compared the classical nucleation theory with the density functional theory for heterogeneous nucleation of a van der Waals fluid on aerosol-like particles. The comparison showed that the capillary approximation incorporated in CNT overestimates the effect of line tension on the work of formation of critical nuclei. Nevertheless, the CNT predictions that incorporate the line tension effect were considerably better than the predictions of the original CNT. Checco *et al.*[20] and Quere,[21] using direct observations of the heterogeneous nucleation on plane surfaces, found that the contact angle at small droplet sizes decreases due to the heterogeneity of the solid and that the line tension effect is completely masked by the surface

[a)]Author to whom correspondence should be addressed. Electronic mail: anca.hienola@helsinki.fi

heterogeneity. While these observations might be applicable for the above system consisting in plane macroscopic solid surface and droplets of 200 nm–2 μm diameter, for our system with 7–15 nm diameter spherical solid particles and critical clusters of about same size, the concept of line tension becomes relevant. Our calculations reveal the inadequacy of the classical heterogeneous nucleation theory in describing the experimental results for *n*-nonane, *n*-propanol, and *n*-nonane+*n*-propanol mixture nucleating on silver particles. The CNT predictions are flawed, giving much larger critical supersaturations than the experimentally observed ones, even if the contact angle is assumed to be zero. However, when we consider the combined effects of properly described negative line tension and microscopic contact angle, the theoretical calculations reconcile with the experimental data.

This paper suggests that the classical heterogeneous nucleation theory can become valid when the interactions between phases are taken into account. The agreement between theory and experiments can be fully accounted by the inclusion of line tension and microscopic contact angle.

The outline of the paper is as follows. In Sec. II we describe briefly the classical heterogeneous nucleation theory with and without the line tension and we outline the way of calculating interfacial tensions and contact angles. Section III is devoted to the results of the classical nucleation theory for unary and binary heterogeneous nucleations of *n*-nonane and *n*-propanol on silver particles, the calculations of the line tension and microscopic contact angles, sensitivity analysis, and the effect of silver particle polydispersity. In the last section we will present the overall conclusions.

II. THEORETICAL CONSIDERATIONS

In the classical nucleation theory, the critical cluster formation rate is given by[10]

$$J = K \exp\left(-\frac{\Delta G^*}{kT}\right), \tag{1}$$

where K is a kinetic factor and ΔG^* is the Gibbs free energy of formation of the critical embryo. It is assumed that the seed particle is a sphere with radius R and the embryo is a portion of a sphere (Fig. 1) with volume V, surface S, and radius r. Henceforth, we denote the parent phase (vapor) with subscript 1, the embryo with 2, and the substrate with 3.

The free energy of formation is[10]

$$\Delta G = \Delta G_{12} V + \sigma_{12} S_{12} + (\sigma_{23} - \sigma_{13}) S_{23}, \tag{2}$$

where ΔG_{12} represents the free energy difference per unit volume of the liquid phase between matter in phase 2 and the matter in phase 1, σ_{ij} is the surface free energy between phases i and j, and S_{ij} is the surface area of the interface. We define here the critical cluster as the cluster for which the derivatives of ΔG with respect to the numbers of molecules in the cluster vanish. The radius of the critical cluster is given—as in the case of homogeneous nucleation—by Kelvin equation,

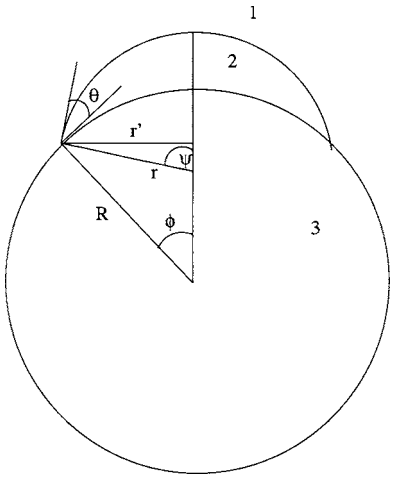

FIG. 1. Sketch of the cross section of a cap-shaped liquid embryo 2 of radius r in equilibrium with the vapor phase 1 on a spherical seed particle 3 of radius R. The liquid embryo forms a contact angle θ with the seed particle.

$$r^* = \frac{2\sigma_{12} v_l}{kT \ln(P_l/P_{\mathrm{sat},l})}, \tag{3}$$

where k is Boltzmann constant, T is the temperature, v_l is the partial molar volume of species l, P_l is the ambient partial pressure of free molecules of species l, and $P_{\mathrm{sat},l}$ represents the equilibrium vapor pressure of species l above a flat solution surface. The formation energy of the critical cluster can be calculated from

$$\Delta G^* = \frac{2\pi r^{*2} \sigma_{12}}{3} f(m,x), \tag{4}$$

with the geometrical factor

$$f(m,x) = 1 + \left(\frac{1-mx}{g}\right)^3 + x^3\left(2 - 3\left(\frac{x-m}{g}\right) + \left(\frac{x-m}{g}\right)^3\right) + 3mx^2\left(\frac{x-m}{g} - 1\right), \tag{5}$$

and

$$g = \sqrt{1 + x^2 - 2mx}, \tag{6}$$

where $m=\cos(\theta)$, θ is the contact angle, $x=R/r^*$, and r^* is the radius of the critical cluster. The nucleation rate, Eq. (1), depends on the contact angle through the free energy of formation of the critical embryo, Eq. (4).

When taking into account the line tension effect, the Gibbs free energy becomes (e.g., Ref. 18)

$$\Delta G = \Delta G_{12} V + \sigma_{12} S_{12} + (\sigma_{23} - \sigma_{13}) S_{23} + 2\pi R \tau \sin\phi, \tag{7}$$

where $2\pi R \sin\phi$ is the length of the contact line and τ is the line tension at the triple phase boundary between the embryo, substrate, and the vapor phase. The resulting height of the nucleation barrier becomes[18]

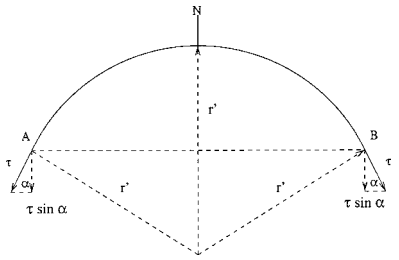

FIG. 2. The line tension of a curved three phase contact line of radius r'. The tension τ acts along the tangents to the curved line, yielding a force $2\tau \sin \alpha / l$.

$$\Delta G^* = \frac{2\pi r^{*2}\sigma_{12}}{3} f(m,x) - \frac{\tau}{R \tan \phi} S_{23} + 2\pi R \tau \sin \phi. \quad (8)$$

From Eq. (8) it can be seen that a positive line tension will increase the critical Gibbs free energy, which consequently will lead to lower nucleation rates. On the other hand, a negative value of the line tension will decrease the Gibbs free energy and will account for higher nucleation rate values. This can be easily demonstrated by showing that the absolute value of $2\pi R\tau \sin \phi$ is larger than the absolute value of $(\tau/R \tan \phi)S_{23}$, where the surface S_{23} is obtained from the geometry in Fig. 1 as $S_{23}=2\pi R^2(1-\cos \phi)$. Scheludko *et al.*[22] examined the concept of negative line tension which explained very well the experimental results for water nucleation on hexadecane. The angle ϕ (Fig. 1) is given by

$$\cos \phi = \frac{R - r \cos \theta}{R^2 + r^2 - 2Rr \cos \theta}. \quad (9)$$

The microscopic contact angle θ is different from the macroscopic contact angle θ_∞ for a sufficiently large radius of a contact line defined by Young's equation,

$$\cos \theta_\infty = \frac{\sigma_{13} - \sigma_{23}}{\sigma_{12}}. \quad (10)$$

It is important to explain at this point what a "sufficiently large radius" means in practice. Marmur and Krasovitski[23] defined this radius of the contact line as the threshold radius above which the absolute difference between the macroscopic and microscopic contact angles is less than 1°, based on the fact that 1° is the lower limit of experimental resolution in contact angle measurements. This means that for any radius of the contact line above the threshold radius, the effect of line tension is negligible.

To derive generalized Young's equation including line tension,[24] we consider a small arc of a curved contact line with length $\breve{AB}=l$, radius r', and line tension τ (Fig. 2). Due to the action of line tension, a force $(2\tau/l)\sin \alpha$ will act upon the arc of length $2\alpha r'$, where α is the angle between the direction N and the tangent to the circle in the point A or B. The force is found by making $\alpha \to 0$,

$$\sigma_\tau = \lim_{\alpha \to 0} \frac{2\tau \sin \alpha}{2\alpha r'} = \frac{\tau}{r'}. \quad (11)$$

If the effect of line tension is included in the derivation of Young's equation, the force σ_τ must be added to the balance of forces along the perimeter of the three phase contact line,

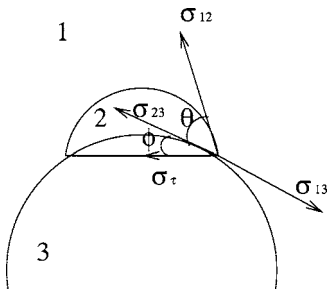

FIG. 3. The force balance representation along the perimeter of the three phase contact line. In this case the tension σ_τ has been added to the balance of forces. σ_{ij} (with $i, j=1,2,3$, $i \neq j$, 1=vapor, 2=liquid, 3=solid) are the interfacial tensions, θ is the contact angle, and Φ is the angle between the plane of the three phase contact line and the solid-liquid interface.

$$\overline{\sigma_{12}} + \overline{\sigma_{23}} + \overline{\sigma_{13}} + \overline{\sigma_\tau} = 0, \quad (12)$$

where the overline denotes vector. According to Fig. 3, the balance along the tangent of the surface of the seed particle gives

$$\sigma_{13} - \sigma_{23} - \sigma_{12} \cos \theta - \sigma_\tau \cos \phi = 0. \quad (13)$$

Using Eq. (11) and the geometry in Fig. 1, Eq. (13) becomes

$$\sigma_{13} - \sigma_{23} - \sigma_{12} \cos \theta - \frac{\tau}{R \tan \phi} = 0. \quad (14)$$

The microscopic contact angle as a function of line tension will take the form

$$\cos \theta = \cos \theta_\infty - \frac{\tau}{\sigma_{12} R \tan \phi}, \quad (15)$$

where we have used Eq. (10) to eliminate the interfacial tensions σ_{13} and σ_{23}. Equation (15) is known as the generalized Young equation.

The macroscopic contact angle has been measured for a limited number of solid-liquid pairs. Here we present a method for calculating the macroscopic contact angle of a certain solid with various liquids when the contact angle with one liquid is known. Equation (15) contains only three measurable quantities, the macroscopic contact angle θ_∞, the radius of the nucleating particle R, and the surface tension of the liquid σ_{12}. The calculation of solid-liquid and solid-vapor interfacial tensions from a measured macroscopic contact angle of a liquid with a known surface tension starts with Young's equation [Eq. (10)]. Several methods are available for calculating the solid-vapor interfacial tension when the contact angle is known. A very simple way is to consider the work of adhesion W_{23} per unit area of a solid-liquid pair. W_{23} is given by Young-Dupré equation,

$$W_{23} = \sigma_{12} + \sigma_{13} - \sigma_{23}. \quad (16)$$

In order to obtain σ_{23} and σ_{13}, a second equation describing the work of adhesion is needed. For example, a free work of adhesion for a liquid-solid pair was proposed[25] as the geometric mean of the free energy of cohesion of solid-solid W_{33} and the work of cohesion for liquid-liquid W_{22} as

$$W_{23} = \sqrt{W_{22}W_{33}}. \tag{17}$$

The work of cohesion is defined as the work done in dividing a homogeneous liquid per parting surface produced. As during division two individual parting surfaces are produced, the work of cohesion can be calculated from the surface tension as $W_{22}=2\sigma_{12}$ and $W_{33}=2\sigma_{13}$. The solid-liquid work of adhesion becomes

$$W_{23} = 2\sqrt{\sigma_{12}\sigma_{13}}. \tag{18}$$

From Eqs. (16) and (18) we obtain an expression for the solid-liquid interfacial tension,

$$\sigma_{23} = \sigma_{12} + \sigma_{13} - 2\sqrt{\sigma_{12}\sigma_{13}}, \tag{19}$$

known as Rayleigh-Good equation. Coupling Eq. (19) with Young's equation (10) results in

$$\cos\theta_\infty = -1 + 2\sqrt{\frac{\sigma_{13}}{\sigma_{12}}}. \tag{20}$$

If we take into account the deviations from the geometric mean, an interaction parameter Φ must be introduced in Eq. (17), leading to

$$\cos\theta_\infty = -1 + 2\Phi\sqrt{\frac{\sigma_{13}}{\sigma_{12}}}. \tag{21}$$

Li and Neumann[26] proposed an empirical expression for the interaction parameter Φ,

$$\Phi = e^{-\beta(\sigma_{12}-\sigma_{13})^2}, \tag{22}$$

where $\beta=0.000\,124\,7$ m^4 mJ^{-2} is a universal constant obtained from a fitting of a large set of experimental data. Equation (21) with Φ expressed as in Eq. (9) is known as the Neumann equation of state for interfacial tension. Although the Neumann equation has been the subject of controversy,[27,28] we applied it in our calculations, first because of its simplicity, second because it does describe well the behavior of many systems, and third because it allows the calculation of vapor-solid interfacial tension σ_{13} and the liquid-solid interfacial tension σ_{23} separately from a limited number of experimental data. However, we must emphasize here that the applicability of Neumann equation to our systems (silver-*n*-nonane, silver-*n*-propanol, and silver-*n*-nonane+*n*-propanol) has not been proven. To the authors knowledge, there are no experimental data concerning the silver surface tension in the vicinity of room temperature. Literature presents a wide spread in the experimental and theoretical data for both solid and liquid silvers, from 0.7 to 2.2 N m^{-1}. However, the data for solid silver surface tension are all in the proximity of the melting point and cannot be extrapolated down to the temperature of the data we analyze (280 K). Therefore, we calculated the solid silver surface tension using Eq. (20) and Neumann equation of state for comparison.

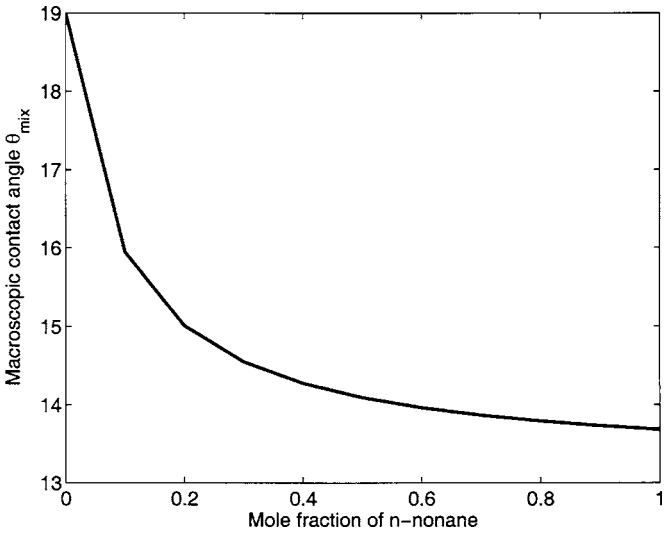

FIG. 4. The macroscopic contact angle (degrees) of the *n*-nonane–*n*-propanol mixture on silver substrate as a function of *n*-nonane mole fraction.

III. RESULTS AND DISCUSSION

A. Macroscopic contact angle for *n*-nonane and *n*-nonane–*n*-propanol on silver

The only available measured macroscopic contact angle for silver substrate found in literature at a temperature close to 280 K is presented by Wagner *et al.*[11] for silver–*n*-propanol system with the value of $\theta_\infty=19°$. With the knowledge of this contact angle and the surface tension of propanol (e.g., Ref. 29) we were able to calculate the solid silver surface tension σ_{13}. Neumann equation of state gave a value of 23.55×10^{-3} N m^{-1} while Eq. (20) resulted in a value of 23.57×10^{-3} N m^{-1}. Given the small difference between the results and the simplicity of Eq. (20), the latter has been used subsequently in our calculations. Using again Eq. (20), but for a different substance (i.e., *n*-nonane) with a known liquid surface tension,[29] we are now able to find the macroscopic contact angle between silver and *n*-nonane. Denoting σ_k and θ_k ($k=n,p$, where $n=n$-nonane and $p=n$-propanol) the surface tensions and the macroscopic contact angles, respectively, the macroscopic contact angle for *n*-nonane on silver can be calculated as

$$\cos\theta_n = -1 + \sqrt{\frac{\sigma_p}{\sigma_n}}(\cos\theta_p + 1). \tag{23}$$

The macroscopic contact angle obtained for *n*-nonane on silver substrate at 280 K was 13.63°. A similar reasoning has been applied for *n*-nonane+*n*-propanol system, with the surface tension of the mixture from Ref. 29. In this case, the macroscopic contact angle of the mixture on silver substrate is a function of the composition, as shown in Fig. 4.

B. Experimental heterogeneous nucleation and data fitting

The experimental data for unary and binary heterogeneous nucleation of *n*-nonane and *n*-propanol on monodispersed silver particles are given in Ref. 30. In this work, the investigation of heterogeneous nucleation was performed by

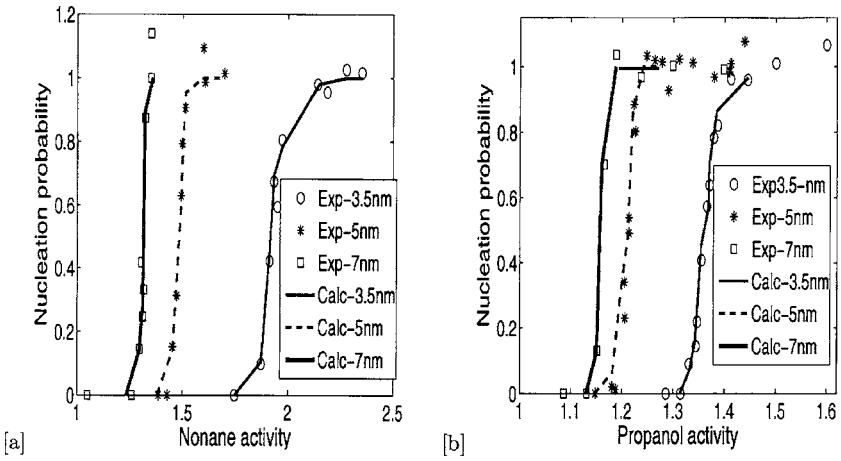

FIG. 5. The nucleation probability vs gas phase activity of (a) *n*-nonane and (b) *n*-propanol. The theoretical prediction is represented by lines and the experiments by squares (for 7 nm radius seed particle), stars (for 5 nm radius seed particle), and circles (for 3.5 nm radius seed particle).

means of the constant-angle Mie scattering for determination of particle number concentration and particle growth.[31] The activation of the nanoparticles was observed in a fast expansion chamber. Measurements of unary heterogeneous nucleation were performed for silver particles with geometric mean radii of 3.5, 5, and 7 nm at constant temperature of 280 K. Binary heterogeneous nucleation on 3.5 and 5 nm radius silver particles was observed for several *n*-nonane:*n*-propanol vapor mixing ratios. The vapor mixtures were obtained by quantitative evaporation from corresponding liquid mixtures with *n*-nonane mass fractions of 0.182, 0.309, 0.385, 0.472, and 0.641.

The thermodynamical data for *n*-nonane, *n*-propanol, and their mixture needed for the calculations have been discussed in detail in our previous paper concerning the homogeneous nucleation of *n*-nonane–*n*-propanol.[29]

To obtain quantitative estimates for the microscopic contact angle θ and the line tension τ, the heterogeneous classical nucleation theory corrected with line tension was fitted to the experimental data. The experiments provide the gas phase activities of *n*-nonane and *n*-propanol and the corresponding nucleation probabilities. The nucleation probability in a time period t is defined as

$$P = 1 - \exp(-J_{\text{het}}t), \tag{24}$$

where J_{het} is the nucleation rate per preexisting particle per unit time. As input we used the gas phase activities. The gas phase activity of a certain compound is defined as the ratio between its ambient vapor pressure and the saturation vapor pressure over a flat surface of pure liquid.[32]

The microscopic contact angle [and in connection the line tension τ which is related to θ by Eq. (15)] was varied in a one parameter fit procedure until the calculated nucleation probabilities were superimposed on the experimental ones. Such fitting was performed over all of the data sets described above. The results of the fitting procedure are presented in the next two sections.

C. Unary systems

The fitted nucleation probabilities are presented in Fig. 5 together with the experimental data from Winkler.[30] The slopes of the nucleation probability curves agree well for both systems and for all seed particle diameters. The estimated values for the microscopic contact angle for both *n*-nonane and *n*-propanol on silver substrate are presented in Fig. 6. The contact angle is found to depend linearly on the cluster radius and it is also a function of the seed particle size. Figure 7 depicts the estimated line tension values as a function of cluster radius. For both of the systems the line tension is negative and depends also on the seed particle diameter. This result comes in agreement with the theoretical findings of Marmur and Krasovitski[23] who investigated the line tension on micro- and nanospheres. Figure 8 shows the formation free energy of the critical cluster $\Delta G^*/kT$ versus propanol activity for a silver particle radius of 5 nm. The upper curve represents the Gibbs free energy based on standard classical theory while the lower curve is calculated by taking into account the line tension effect. When we compare the nucleation barriers calculated with and without line tension, we find that the original classical theory seriously overestimates the height of the nucleation barrier. A negative line tension explains the decrease in the work of formation of the embryos on silver substrate and consequently an increase in

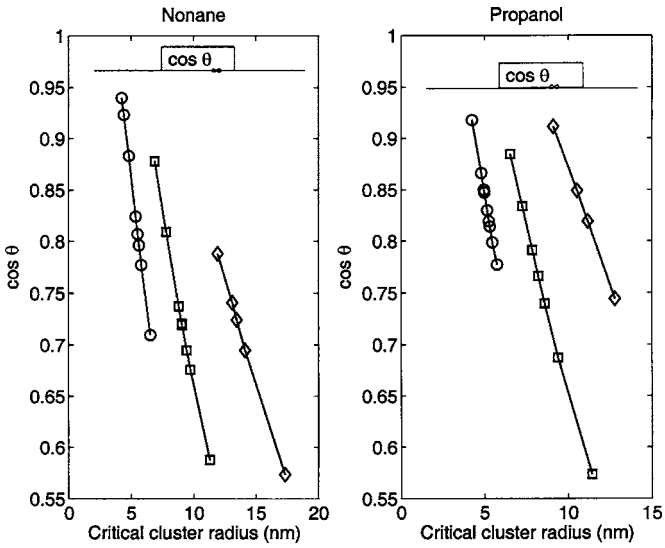

FIG. 6. The cosine of the contact angle vs cluster radius for *n*-nonane and *n*-propanol. The curves in each figure correspond to the different seed particle sizes: circles, 3.5 nm particle radius; squares, 5 nm particle radius; diamonds, 7 nm particle radius. The corresponding values for the macroscopic contact angle are presented graphically by the horizontal lines at the top of the figure.

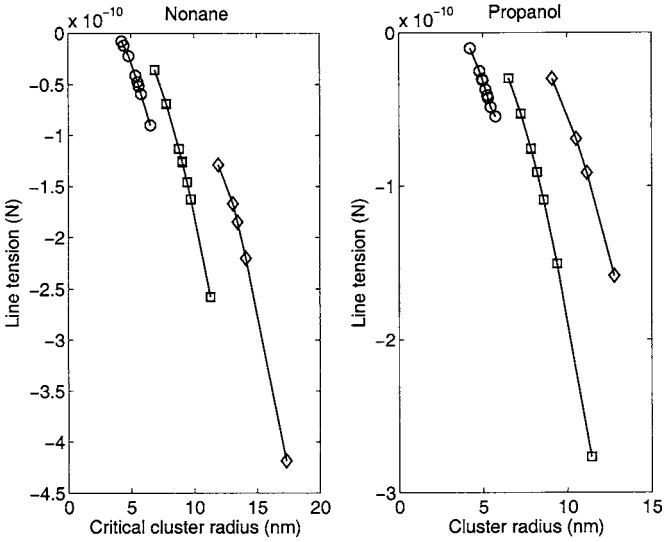

FIG. 7. The line tension vs cluster radius for *n*-nonane and *n*-propanol. The curves in each figure correspond to the different seed particle radii, as specified for Fig. 6.

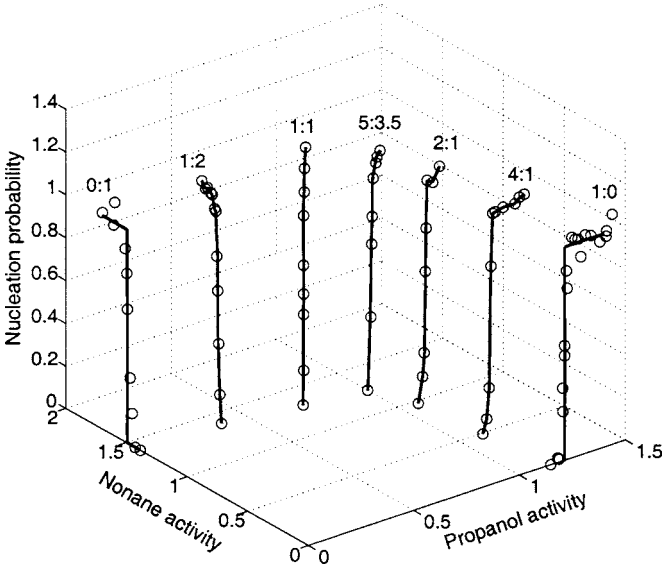

FIG. 9. A three-dimensional representation of the nucleation probability of *n*-nonane–*n*-propanol mixture on 5 nm radius seed particle. Circles: experimental data; lines: CNT corrected with line tension predictions. The numbers on top of each curve show the *n*-nonane:*n*-propanol mixing ratios. For comparison, the limiting cases (0:1 and 1:0) are presented.

nucleation rate. Similar figures can be obtained for the 3.5 nm seed particle radius and also for *n*-nonane.

D. Binary systems

The experimental heterogeneous nucleation probabilities for 3.5 and 5 nm particles have been used to fit the classical theory and to obtain the unknown contact angle and line tension. As an example, in Fig. 9 the experimental and the fitted nucleation probabilities for 5 nm particles are presented for seven different mixing ratios, including the unary systems, as a function of *n*-nonane and *n*-propanol gas phase activities. For the binary system, the computed nucleation probabilities follow nicely the experimental data. An analogous behavior was found also for 3.5 nm silver particles.

The computed onset activities corresponding to a heterogeneous nucleation probability of 0.5 for all nucleating particle sizes are presented in Fig. 10 as a function of *n*-nonane and *n*-propanol activities in gas phase. For clarity, the experimental points have not been plotted, but they overlap the fitted ones. The onset curves for 3.5 and 5 nm particles have a similar trend and clearly depend on the nucleating particle size. The shape of the curve bending away from origin shows that the substances hardly conucleate, which is true also in the case of homogeneous nucleation.[29]

The contact angle and line tension values required for the calculated nucleation probabilities to fit the experimental data are presented in Fig. 11. The cosine of the contact angle depends on the seed particle size and displays a linear dependence on the cluster radius [Fig. 11(a)]. Furthermore, the angle ϕ is found to be obtuse and accordingly the radius of the cluster is always bigger than the seed particle radius. In all cases, the obtained microscopic contact angle is higher than the macroscopic one. This finding comes in contradic-

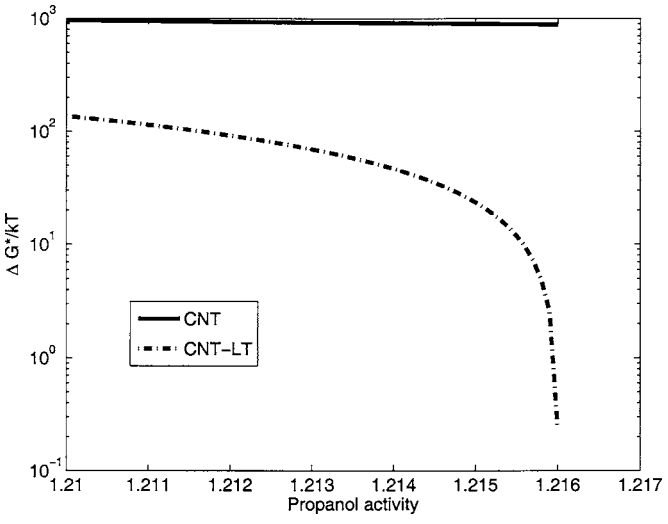

FIG. 8. The critical Gibbs free energy barrier in the case of *n*-propanol on 5 nm radius seed particles. The upper curve represents the prediction of the original CNT, while the lower curve the prediction of CNT corrected with line tension.

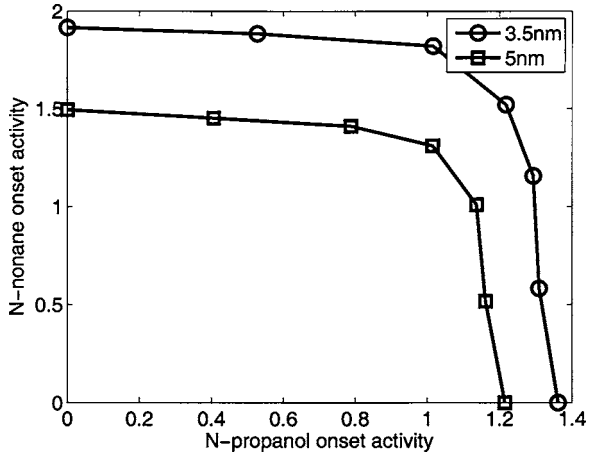

FIG. 10. The theoretical onset activities for heterogeneous nucleation of binary *n*-nonane–*n*-propanol mixtures on silver particles. Experimental points, circles and squares; calculated, lines.

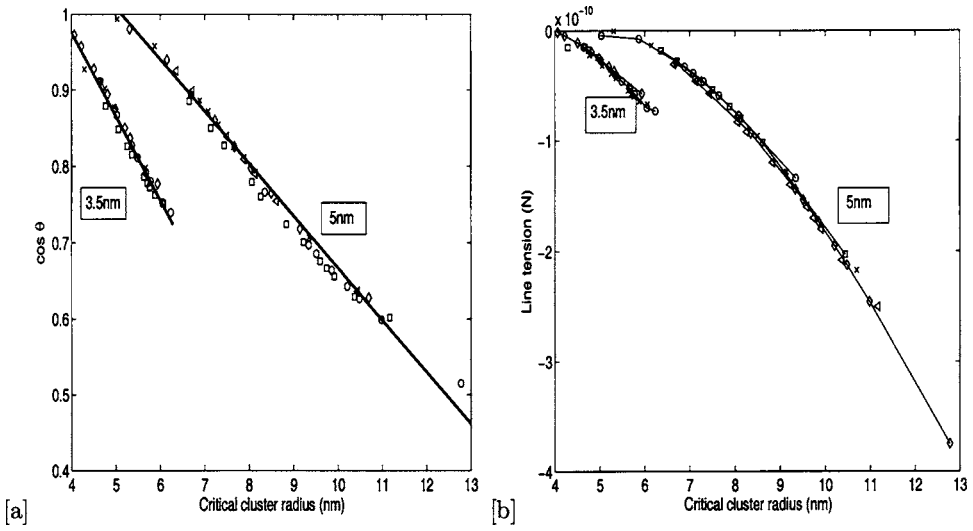

FIG. 11. (a) The cosine of the microscopic contact angle for binary *n*-nonane–*n*-propanol mixtures on silver particles (dots) and the linear fit (line) plotted against the cluster radius. (b) The calculated line tension vs cluster radius. The numbers beside each curve in both figures represent the seed particle radii. Each symbol corresponds to a certain mixing ratio.

tion with the results of Ref. 11 where the fitted contact angle for the same liquid and substrate was found to be much smaller than the macroscopic experimental values. However, the authors did not account for the influence of the line tension in their calculations. Line tension varies with the contact angle θ, the radius of the cluster r, and the radius of the seed particle R. The variation of τ with the cluster and seed particle radii is depicted in Fig. 11(b). The line tension becomes increasingly negative, for example, for a particle of 5 nm radius, three orders of magnitude from -3.4×10^{-13} N at 5.3 nm cluster radius to -3.75×10^{-10} N at 12.77 nm cluster radius. The values for τ are of the same order of magnitude as previous estimations for different systems.[33,34]

Of special interest is the dependence of τ on the microscopic contact angle θ. If our calculations are correct, the line tension should approach zero as we are getting closer to total wetting. Figure 12 shows that for all particle sizes, the line tension converges to zero as the microscopic contact angle decreases which leads us to the conclusion that the calculated parameters τ and θ behave physically correctly. Our findings are in agreement with other experimental data which show that the line tension vanishes at wetting (e.g., Ref. 35) but not fully corroborated by the theoretical predictions for line tension near wetting, which assert that line tension will tend to infinity.[36,37] From the physical point of view, the three phase border line disappears at wetting and a zero value for the line tension looks more plausible than a theoretical infinite line tension.

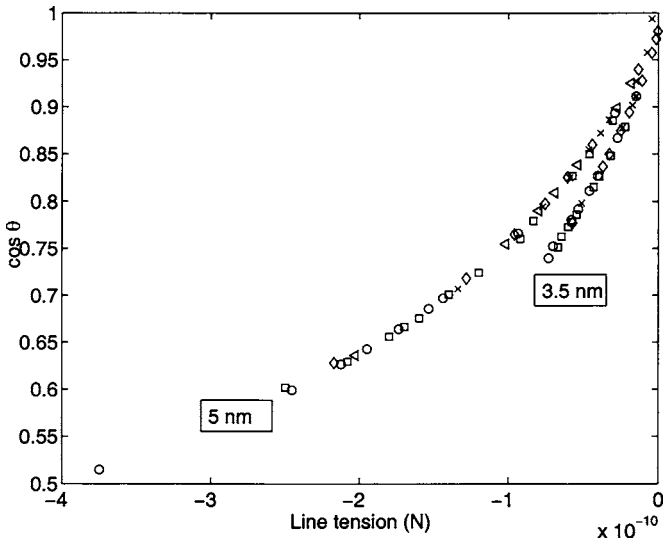

FIG. 12. The cosine of the contact angle vs the line tension. The numbers beside each curve represent the seed particle radii and each symbol corresponds to a certain mixing ratio. The line tension approaches zero as we get closer to total wetting ($\cos\theta=1$).

E. Why is θ larger than θ_∞ ?

It is known that the line tension sign affects the microscopic contact angle of a liquid drop on a solid surface. If we treat the line tension in a Gibbsian way, as a one-dimensional analog of the surface tension, the sources of the excess energy at the triple boundary line are mainly the intermolecular interactions for the molecules located along the line.[38] Some other forces are expected to contribute to the linear excess energy, such as the interfacial tensions, solvation, electrostatic and Lifshiftz–van der Waals forces, etc. Under the influence of these forces, the molecules along the line will tend to move towards a more stable state, motion which will define the sign of the line tension and will disturb the shape of the liquid surface in the vicinity of the triple boundary. This disturbance will then define the microscopic contact angle which becomes different than the macroscopic one.

The deviations from the macroscopic angle are schematically presented in Fig. 13 for a general case of a liquid drop on a plane solid surface for both positive (a) and negative (b) line tensions. A positive line tension tends to fold in the liquid surface near the boundary where the surfaces meet by constricting the length of the contact line. In such case, the microscopic contact angle becomes larger than the macroscopic one. A negative line tension could be regarded as a force pushing the edges of the liquid droplet apart, increasing so the length of the contact line. Evidently, in this case the microscopic contact angle will be smaller than the macroscopic one.

A similar reasoning can be applied for a drop on a spherical particle. We will consider two cases, both with

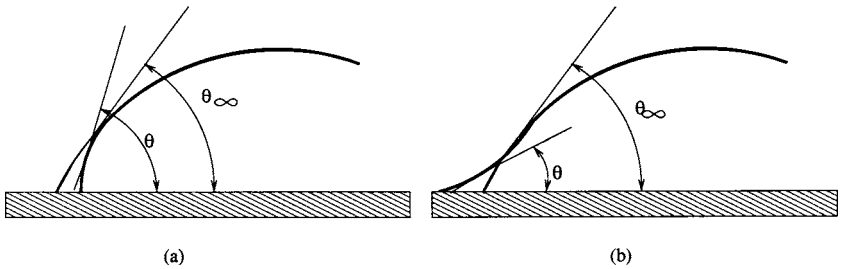

FIG. 13. Deviations from the macroscopic contact angle for a liquid drop on a flat solid surface: (a) a positive line tension decreases the perimeter of the contact line and leads to $\theta > \theta_\infty$; (b) a negative line tension increases the perimeter of the contact line leading to $\theta < \theta_\infty$.

negative line tension: (a) the liquid drop smaller than the solid particle ($r < R_p$) and (b) the liquid droplet covers more than a half of the spherical particle (such as our particular case). These cases are schematically presented in Fig. 14. Having a negative line tension, the line will tend to increase in size and consequently to move towards the equator of the particle. This means that, in the first case, the line tension will relax the liquid surface and decrease the microscopic contact angle, while for the second case the line will fold in the liquid surface, and by doing so increasing the value of the microscopic contact angle above the value of the macroscopic one. This shows that our findings do not come in contradiction with the results found in literature, but they represent just a particular case of a general rule.

However, very little is known about the shape of liquid drops in vicinity of the triple phase boundary and therefore more experimental and theoretical studies are needed for a better understanding of such an interesting phenomenon.

F. General expressions for line tension and contact angle

It would be useful to find a theoretical expression that correlates line tension with a measurable parameter, but deriving this kind of relation is not trivial. Using Eqs. (9) and (15) we can express the line tension as

$$\tau = \frac{rR \sin\theta}{R - r\cos\theta}\sigma_{12}(\cos\theta_\infty - \cos\theta). \tag{25}$$

Here R, σ_{12}, and θ_∞ are measurable quantities and the critical cluster radius r can be calculated relatively easily from homogeneous nucleation theory for any mixing ratio. The only parameter that has to be determined is the microscopic contact angle θ. The cosine of the contact angle is a linear function of the radius of the critical cluster, but, as it can be seen from Fig. 11(a), it is also a function of the seed particle size. The latter dependency can be graphically eliminated if we plot the cosine of the contact angle against r^*/R. The two lines corresponding to the two seed particle radii will collapse onto one single line, as in Fig. 15, and it can be expressed simply as

$$\cos\theta = a\frac{r^*}{R} + b, \tag{26}$$

where $a=-0.32$ and $b=1.3$ for propanol and $a=-0.36$ and $b=1.4$ for nonane. Although the lines are very close to each other, a common equation cannot be used for both substances for predicting nucleation rates and probabilities, due to the fact that the latter ones are very sensitive to small variations in the microscopic contact angle. Relation (26) allows us to calculate the microscopic contact angle for any seed particle radius and subsequently, according to Eq. (25), the line tension. However, the above expressions can be used only for unary heterogeneous nucleation of *n*-nonane and *n*-propanol on silver substrate. It is expected that the microscopic contact angle and line tension will differ for different substrates and/or nucleating substances.

The applicability of Eq. (25) was tested by calculating the onset activities for different sizes of the seed particles for both propanol and nonane unary systems. For example, the onset activities for propanol for seed particle from 10 down to 3.7 nm were plotted against the inverse of the diameter

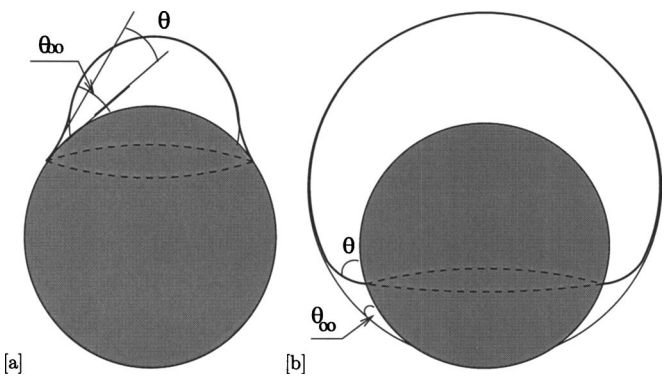

FIG. 14. Deviations from the macroscopic contact angle for a liquid drop on a spherical solid particle with negative line tension: (a) $r < R_p$; (b) $r > R_p$. See the explanation within the text.

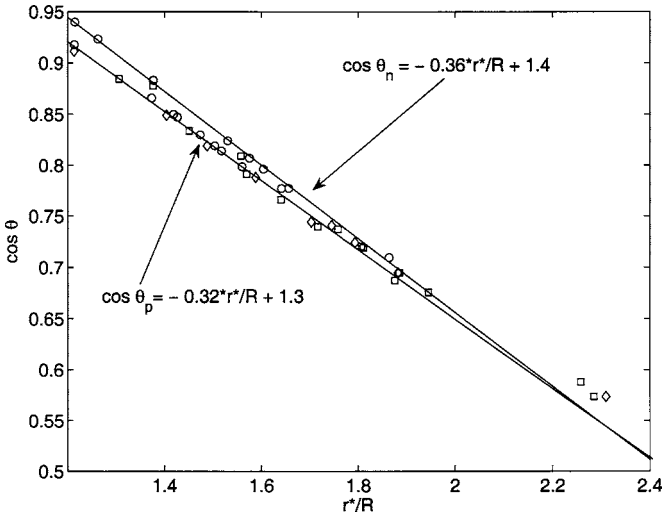

FIG. 15. The cosine of the contact angle vs r^*/R for both nonane (upper curve) and propanol (lower curve). Different symbols represent different seed particle radii. The solid lines represent the fitting over all points for each condensable vapor. The fitted equations are also presented.

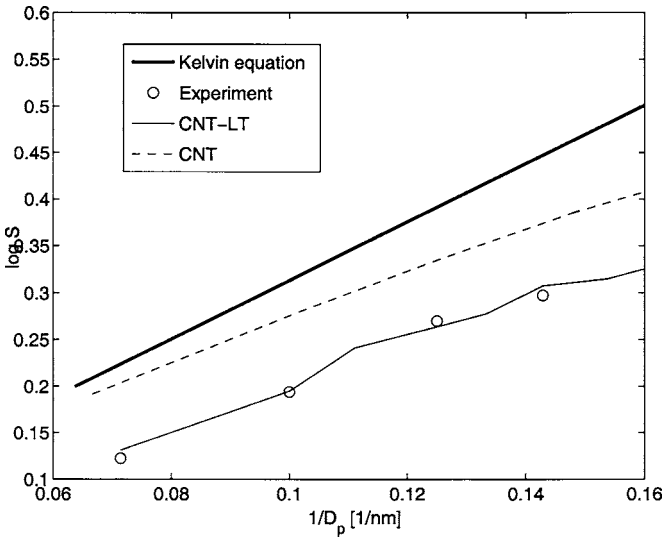

FIG. 16. Onset saturation ratio S vs. inverse of seed particle diameter compared to Kelvin equation (thick line) and Fletcher theory (dashed line) for n-propanol. Circles correspond to the experimental data and the thin line represents the Fletcher theory corrected with line tension. For the calculated points down to 3.7 nm diameter, Eq. (25) has been used.

$1/D_p$, together with the Kelvin equation and the Fletcher theory not corrected with line tension and macroscopic contact angle assumed zero (Fig. 16). The experimental data for 3.5, 5, and 7 nm radii are shown for comparison. An experimental point for 4 nm seed particle radius is included as well[11] but was not used in determining the parameters for Eq. (25) and it is shown here only for comparison. The predicted value of the onset activity for 4 nm particle is in good agreement with the experimental value. Similar behavior can be found also for n-nonane.

G. Sensitivity analysis

The final results of our evaluations, namely, microscopic contact angle and line tension, are subject to several uncertainties. These may be related to the numerical tool itself, to the physics of the problem as well as to the experimental errors. Here we will focus on studying the sensitivity of microscopic contact angle and line tension by varying one key value about which there is some uncertainty: the solid silver surface tension.

The solid silver surface tension has been determined by means of Eq. (20), where both propanol surface tension σ_p and the propanol-silver macroscopic contact angle $\cos\theta_p$ are measured parameters. The value found for the solid silver surface tension σ_{13} is 23.55 mN/m. In the following we determine the error introduced by both propanol surface tension and propanol-silver contact angle, at this point without accounting for the accuracy of Eq. (20) itself.

Starting from Eq. (20), we can derive the surface tension of silver as

$$\sigma_{13} = \sigma_p \left(\frac{1+\cos\theta_p}{2} \right)^2. \tag{27}$$

The error in σ_p will be symbolized by $\epsilon\sigma_p$, the error in σ_{13} by $\epsilon\sigma_{13}$, and the error in $\cos\theta_p$ by $\epsilon\cos\theta_p$. The error in σ_{13} can be calculated as

$$\epsilon\sigma_{13} = \left(\left(\frac{\partial\sigma_{13}}{\partial\sigma_p}\epsilon\sigma_p \right)^2 + \left(\frac{\partial\sigma_{13}}{\partial\cos\theta_p}\epsilon\cos\theta_p \right)^2 \right)^{1/2}, \tag{28}$$

where

$$\frac{\partial\sigma_{13}}{\partial\sigma_p} = \left(\frac{1+\cos\theta_p}{2} \right)^2 \text{ and } \frac{\partial\sigma_{13}}{\partial\cos\theta_p} = \sigma_p \left(\frac{1+\cos\theta_p}{2} \right).$$

The term containing the error in σ_p can be neglected, since the values obtained for propanol surface tension are accurate to ±0.01 mN/m. Therefore Eq. (28) simplifies to

$$\epsilon\sigma_{13} = \frac{\partial\sigma_{13}}{\partial\cos\theta_p}\epsilon\cos\theta_p. \tag{29}$$

From experiments by Ortner[39] for contact angle by means of Wilhelmy plate method it can be concluded that an experimental uncertainty in contact angle of ±2° is reasonable. This error in contact angle will lead to an error in the cosine $\epsilon\cos\theta_p = 0.012$.

The uncertainty of the silver surface tension as calculated by Eq. (29) is $\epsilon\sigma_{13} = 2.86\times10^4$ N/m^2, which represents only 1.21% from the initially calculated value. The effect of this very small variation on the final value of microscopic contact angle and line tension is insignificant.

However, because the accuracy of Eq. (20) cannot be quantified, we consider a speculative error of ±5% in the solid silver surface tension. The effect of increasing the silver surface tension by 5% is significant: the subsequently calculated macroscopic contact angle for nonane (taken as an example) on silver leads to $\theta_n = 0$ (total wetting). The calculated values for the microscopic contact angle decrease by only 2%–4%, while the line tension absolute values decrease about 12%. When decreasing the surface tension by 5%, the macroscopic contact angle for nonane on silver increases about 10°, leading to an increase of the microscopic contact angle of about 3%–6% and also an increase of the absolute value of the line tension of 10%. Nevertheless, the line tension remains well within the same order of magnitude in all cases. Figures 17 and 18 present the resulting microscopic contact angles and line tension for a variation of the silver surface tension of ±5% together with the originally calculated values (circles) against the nonane gas phase activity.

H. Effect of silver particle polydispersity

In the previous sections, the calculations were based on the assumption of a strictly monodisperse seed particle population. To explore the effect of polydispersity, we considered the actual experimental particle size distribution, as obtained from electrical mobility spectrometer (EMS) measurements, with an average geometric standard deviation of 1.06. We found that the nucleation probability calculated with the help of Eq. (25) depends profoundly on the accuracy of the parameters a and b. For example, in the case of propanol vapors, for a size distribution around 3.5 nm seed particles, the parameters a and b must have the exact values of −0.318 and 1.3, respectively, for a perfect match with the experimental data, while for a distribution around 10 nm $a=-0.318\,37$ and $b=1.2895$. If the values of $a=-0.32$ and $b=1.3$ are used, the resulting nucleation probabilities will be overestimated for

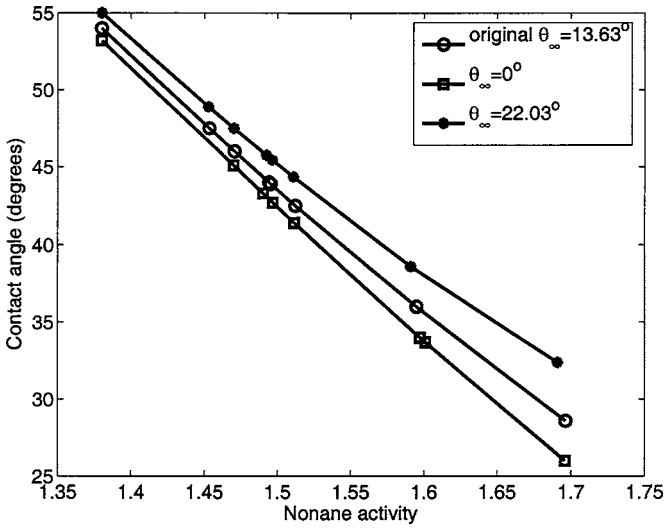

FIG. 17. Sensitivity analysis: microscopic contact angle of nonane on 5 nm radius silver particles against nonane gas phase activity. The circles correspond to the originally calculated macroscopic contact angle, squares to a macroscopic contact angle 0, obtained by increasing the silver surface tension with 5%, and the stars to a contact angle of 22.03°, corresponding to a decrease in silver surface tension of 5%.

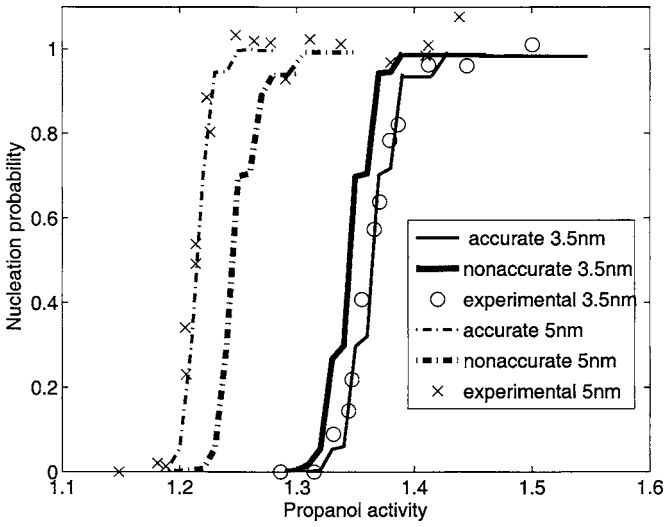

FIG. 19. Experimental and calculated nucleation probabilities vs propanol gas phase activities for particle size distribution centered at 3.5 nm (solid lines) and 5 nm (dash-dotted lines). The calculated probabilities show a very strong dependence on the accuracy of parameters a and b from Eq. (26).

3.5 nm and underestimated for 5 nm size distributions, as depicted in Fig. 19. This sensitivity can be attributed to the fact that the energy barrier, as given in Eq. (7), is a very strong function of the microscopic contact angle θ. The dependence of the first term in Eq. (7) on θ is not pronounced, but the next two terms will respond to small variations of the macroscopic contact angle via line tension τ and angle ϕ. Figure 20 demonstrates the sensitivity of the energy barrier height as a function of the vapor activity for a size distribution centered at 3.5 nm calculated with contact angle from Eq. (26), with all the above listed values for parameters a and b.

IV. CONCLUSIONS

We have explored the predictions of CNT corrected with line tension for the heterogeneous nucleation of n-nonane, n-propanol, and their mixture on silver particles of three different radii. As a general conclusion, the corrected classical heterogeneous nucleation probabilities show a strong dependence on the value of line tension. We report here the values for microscopic contact angle and line tension required to fit the classical nucleation theory to experimental data. We also study the dependence of microscopic contact angle and line tension on the cluster and seed particle radii. It has been found that, for the particular systems considered, agreement with the experimental data can be only achieved if the line tension has a negative value. In this case the theory predicts that the microscopic contact angle θ is not necessarily smaller than the macroscopic one θ_∞, as it has been assumed until now in the literature.[11,18] With angle ϕ obtuse ($\phi > 90°$), we obtain an even smaller nucleation barrier and consequently a higher nucleation rate than with $\phi < 90°$ and $0 < \theta < \theta_\infty$. Using the values obtained for microscopic con-

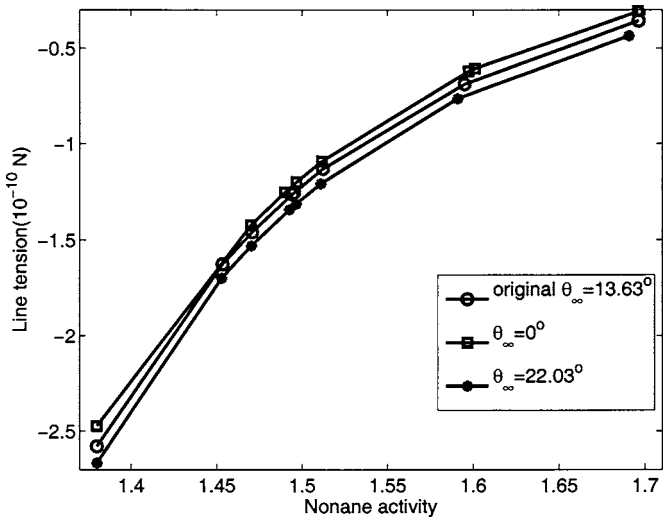

FIG. 18. Sensitivity analysis: line tension of nonane on 5 nm radius silver particles against nonane gas phase activity. Symbols as described in Fig. 17.

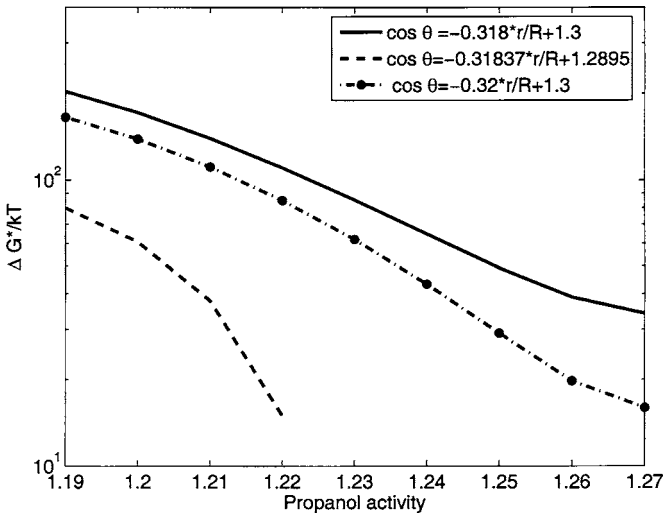

FIG. 20. The energy barrier vs propanol gas phase activities for a particle size distribution centered at 3.5 nm calculated using Eq. (26) with slightly different parameters, as described in the text.

tact angle, we were able to derive a simple equation describing the dependence of cosine of the microscopic contact angle m as a function of the seed particle and cluster radii, namely, Eq. (25). However, its applicability is limited only to strictly monodisperse preexisting particle size distribution. When the experimental width of the size distribution is taken into account, the calculated nucleation probabilities become pronouncedly sensitive to the accuracy of the parameters a and b of Eq. (26). This study clearly illustrates the importance of understanding the concept of line tension in heterogeneous nucleation. We have also shown that heterogeneous nucleation experiments allow to derive meaningful empirical values for the microscopic contact angle and line tension.

ACKNOWLEDGMENTS

Academy of Finland is gratefully acknowledged for financial support. Part of this work was supported by Fonds zur Foerderung der Wissenschaftlichen Forschung, Austria, Project No. P16958-N02.

[1] M. Kulmala, K. E. J. Lehtinen, and A. Laaksonen, Atmos. Chem. Phys. **6**, 787 (2006).
[2] M. Lazaridis, M. Kulmala, and A. Laaksonen, J. Aerosol Sci. **22**, 823 (1991).
[3] M. Kulmala, A. Lauri, H. Vehkamäki, A. Laaksonen, D. Petersen, and P. E. Wagner, J. Phys. Chem. B **105**, 11800 (2001).
[4] P. Hamill, R. P. Turco, , C. S. Kiang, O. B. Toon, and R. C. Whitten, J. Aerosol Sci. **13**, 561 (1982).
[5] N. Fletcher, J. Atmos. Sci. **26**, 1266 (1969).
[6] B. Z. Gorbunov and N. A. Kakutkina, J. Aerosol Sci. **13**, 21 (1982).
[7] D. W. Lee, P. K. Hopke, D. H. Rasmussen, H. C. Wang, and R. Mavliev, J. Phys. Chem. B **107**, 13813 (2003).
[8] A. Laaksonen, V. Talanquer, and D. W. Oxtoby, Annu. Rev. Phys. Chem. **46**, 489 (1995).
[9] E. Zapadinsky, A. Lauri, and M. Kulmala, J. Chem. Phys. **122**, 114709 (2005).
[10] N. Fletcher, J. Chem. Phys. **29**, 572 (1958).
[11] P. Wagner, D. Kaller, A. Vrtala, A. Lauri, M. Kulmala, and A. Laaksonen, Phys. Rev. E **67**, 021605 (2003).
[12] J. Faraudo and F. Bresme, J. Chem. Phys. **118**, 6518 (2003).
[13] D. Platikanov, M. Nedyalkov, and A. Scheludko, J. Colloid Interface Sci. **75**, 612 (1980).
[14] D. Platikanov, M. Nedyalkov, and V. Nasteva, J. Colloid Interface Sci. **75**, 620 (1980).
[15] P. Kumar, G. Gompper, and R. Lipowsky, Phys. Rev. Lett. **86**, 3911 (2001).
[16] R. Gretz, Surf. Sci. **5**, 239 (1966).
[17] G. Navascues and L. Mederos, Surf. Technol. **17**, 79 (1982).
[18] M. Lazaridis, J. Colloid Interface Sci. **155**, 386 (1993).
[19] K. Padilla and V. Talanquer, J. Chem. Phys. **114**, 1319 (2001).
[20] A. Checco, J. P. Guenoun, and J. Daillant, Phys. Rev. Lett. **91**, 186101 (2003).
[21] D. Quere, Nat. Mater. **3**, 79 (2004).
[22] A. Scheludko, V. Chakarov, and B. Toshev, J. Colloid Interface Sci. **82**, 83 (1981).
[23] A. Marmur and B. Krasovitski, Langmuir **18**, 8919 (2002).
[24] A. Scheludko, B. Toshev, and D. Platikanov, in *The Modern Theory of Capillarity: To the Centennial of Gibbs' Theory of Capillarity*, edited by F. Goodrich and A. Rusanov (Akademie, Berlin, 1981).
[25] L. Girifalco and R. Good, J. Phys. Chem. **61**, 904 (1957).
[26] D. Li and A. Neumann, Adv. Colloid Interface Sci. **39**, 299 (1992).
[27] R. Johnson and R. Dettre, Langmuir **5**, 293 (1989).
[28] I. Morrison, Langmuir **5**, 540 (1989).
[29] A. I. Gaman, I. Napari, P. M. Winkler, H. Vehkamäki, P. E. Wagner, R. Strey, Y. Viisanen, and M. Kulmala, J. Chem. Phys. **123**, 244502 (2005).
[30] P. Winkler, Ph.D. thesis, Fakultaet fuer Naturwissenschaften und Mathematik der Universitat Wien, 2004.
[31] P. Wagner, J. Colloid Interface Sci. **105**, 456 (1985).
[32] H. Vehkamäki, *Classical Nucleation Theory in Multicomponent Systems* (Springer, Berlin, 2006).
[33] T. Pompe and S. Herminghaus, Phys. Rev. Lett. **85**, 1930 (2000).
[34] J. Wang, S. Betelu, and B. M. Law, Phys. Rev. E **63**, 031601 (2001).
[35] A. Amirfazli, A. Keshavarz, L. Zhang, and A. W. Neumann, J. Colloid Interface Sci. **265**, 152 (2003).
[36] J. F. Joanny and P. G. De Gennes, J. Colloid Interface Sci. **111**, 94 (1986).
[37] I. Szleifer and B. Widom, Mol. Phys. **75**, 925 (1992).
[38] J. Drelich, Colloids Surf., A **116**, 43 (1996).
[39] R. Ortner, Master's thesis, Universität Wien, Wien, Österreich, 2000.